ELSEVIER

Cement & Concrete Composites 25 (2003) 767–777

Cement & Concrete Composites

www.elsevier.com/locate/cemconcomp

Uniaxial tension test for steel fibre reinforced concrete—a parametric study

Bryan E. Barragán [a], Ravindra Gettu [a,*], Miguel A. Martín [a], Raúl L. Zerbino [b]

[a] *Department of Construction Engineering, Structural Technology Laboratory, Universitat Politècnica de Catalunya, ETSECCPB, Jordi Girona 1-3, Edificio C1, E-08034 Barcelona, Spain*

[b] *CONICET, LEMIT, Universidad Nacional de La Plata, La Plata 1900, Argentina*

Received 5 April 2002; accepted 5 August 2002

Abstract

A RILEM Draft Recommendation was proposed in 2001 for obtaining the stress versus crack opening (σ–w) response of steel fibre reinforced concrete through a uniaxial tension test. The present study analyses the robustness of the recommended test through a parametric study. Furthermore, the methodology is extrapolated to cores extracted from cast elements. Also, the effect of the coring direction with respect to the preferential fibre orientation caused by the compaction procedure is examined. The study demonstrates that the test is robust and representative of the material response, and could be used for determining the σ–w relation of the material that may be needed for comparing the performance of different fibres or for providing input for finite element analysis. No significant influence of the characteristics of the specimen or problems of instability due to the loss of control were encountered. There is some relative rotation between the crack faces but its influence on the σ–w response is expected to be negligible. The parameters obtained from the tests exhibit coefficients of variation of up to 30%, which is mainly attributed to the randomness of the number of fibres bridging the crack, considering the relatively small cross-section of the specimen.

Keywords: Uniaxial tension; Steel fibre; Concrete

1. Introduction

A fundamental aspect of the mechanical performance of steel fibre reinforced concrete (SFRC) is the tensile behaviour and, more specifically, the tensile stress versus crack opening response. This can be characterised through a uniaxial tension test such as that of the recently proposed RILEM Draft Recommendation [1], where a notched cylinder is tested under fixed end conditions. The test is performed under closed-loop control with the average crack opening as the control variable. The recommendation can be considered as the result of previous works that have tested notched prisms and cylinders, under fixed end conditions, to determine the constitutive behaviour of SFRC in tension [2–7]. The constitutive stress-crack opening (σ–w) relationship [8] thus obtained could be used in structural analysis based on fracture mechanics or similar theories, and for deriving toughness parameters that can be incorporated in code-type structural design.

The present study analyses the robustness of the recommended procedure through tests of specimens with different heights and notch depths. Furthermore, the test methodology is also used to determine the response of cores extracted from cast elements. The effect of the coring direction with respect to the preferential fibre orientation caused by the vibration during compaction is examined. Parameters such as relative crack face rotation, effective fibre count and equivalent post-peak tensile strength have been introduced to further analyse the behaviour.

2. Materials and specimen details

Concrete with a characteristic 28-day compressive strength of 30 MPa, containing 40 kg/m^3 of Dramix® RC 80/60 BN hooked-ended collated low carbon steel

* Corresponding author. Tel.: +34-93-401-7354; fax: +34-93-401-1036.

E-mail address: ravindra.gettu@upc.es (R. Gettu).

0958-9465/$ - see front matter © 2002 Elsevier Ltd. All rights reserved.
doi:10.1016/S0958-9465(02)00096-3

Table 1
Composition of the concrete

Components (kg/m^3)	
Cement (CEM I 52.5R)	349
Crushed limestone gravel (5–12 mm)	978
Crushed limestone sand (0–5 mm)	873
Water added	205
Fibres	40
Naphthalene-based superplasticizer dosage (solids/cement ratio, by weight)	0.25%
Water/cement ratio	0.57

Table 2
Properties of the fibres

Properties	
Length	60 mm
Diameter	0.75 mm
Minimum tensile strength	1 GPa
Minimum value of maximum elongation	0.8%

fibres, was used in the study. The concrete composition is given in Table 1 and the properties of the fibres, as specified by the manufacturer, are shown in Table 2.

The test specimens were fabricated from three batches of concrete prepared in a 250 l vertical axis forced-action mixer. The average slump of the fresh concrete was 70 mm and the mean compressive strength obtained from 150×300 mm cylindrical specimens at the average testing age of 70 days was 41.1 MPa.

The RILEM Draft Recommendation [1] specifies a cylinder with a diameter of 150 mm and a height of 150 mm, in which a 15 mm deep notch is cut at mid-height. In the present work, this specimen as well as other modified geometries have been studied. For this purpose, cylinders with 150 mm diameter and two heights, 300 and 450 mm, were cast in rigid moulds and compacted by tamping in three layers. In tests where 150 mm high specimens were used, they were cut from the middle of the 300 mm high specimens. Additionally, prisms of $150 \times 150 \times 600$ mm were cast and compacted by table vibration. After 24 h, all the specimens were demoulded and placed in a fog room (20 °C and 98% R.H.) during 28 days and then stored in laboratory environment until the time of testing. Circumferential notches (of 2.5 mm width) were cut at the mid-height of the specimens, before testing, with a diamond-edged saw.

The different types of specimens used in the tension tests are listed in Table 3. The first series deals with the study of the effect of slenderness (i.e., the height/diameter ratio) over a range of 1–3. The notch depth was maintained as 15 mm, as in the RILEM Recommendation [1]. In the second series, the effect of notch depth was studied with notches of 10–20 mm using cylinders of 150×150 mm. In the third series, tests were performed on cores extracted from the prisms in the vertical (i.e., along the casting direction) and horizontal directions. In each case, at least five specimens were tested.

3. Test details

The tension tests were performed with fixed loading surfaces, as in the RILEM Recommendation [1]. This was achieved by bonding the flat ends of the specimen to the fixed loading plattens of the testing machine using a glue (HBM X60-NP) that needed only about 15 min to cure. One end at a time, starting with the lower end, was glued to the corresponding platten and the adhesive was allowed to cure under a small load (about 1.5 kN). This procedure avoided any misalignment of the specimen with respect to the machine axis.

The tests were performed in an Instron 8500 Plus servo-hydraulic system. They were controlled by means of the average value ($\bar{\delta}$) of the crack mouth opening displacement (CMOD) obtained from three extensometers (of 2.5 mm span and 25 mm gauge length) placed around the specimen at 120° to each other. In the case of the moulded cylinders, three other CMOD measurements around the circumference were also obtained with LVDTs (of 5 mm span) mounted, at 120° to each other, between two rings placed across the notch (see Fig. 1).

The tests were performed with the following $\bar{\delta}$-rate sequence: 5 μm/min up to $\bar{\delta} = 50$ μm, then 100 μm/min up to $\bar{\delta} = 1000$ μm and 500 μm/min then onwards up to $\bar{\delta} = 2000$ μm. All readings were recorded through the data acquisition unit of the testing system using the INSTRON Wavemaker software.

4. Specimen response

The principal objective of the test methodology is the determination of the σ–w curve using the experimentally

Table 3
Specimens used in the uniaxial tension tests

Test series	Variables
Cylinders of 150 mm diameter and notch depth of 15 mm for studying the effect of slenderness	Specimen height: 150, 300, 450 mm
Cylinders of 150 mm diameter and 150 mm height for studying the effect of notch depth	Notch depth: 10, 15, 20 mm
Cored cylinders of 93 mm diameter, 100 mm height and notch depth of 9.3 mm for comparing the responses of moulded and cored specimens	Coring direction: vertical, horizontal

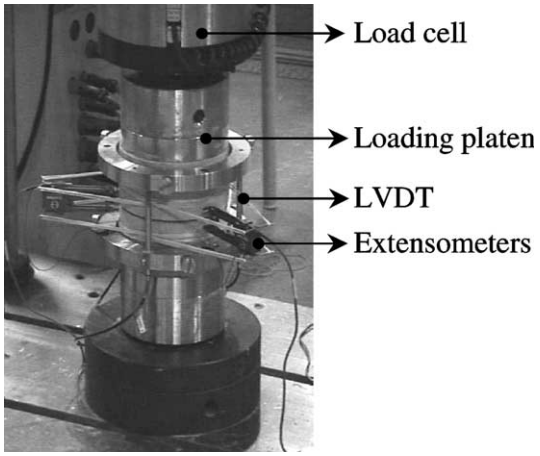

Fig. 1. Test set-up for the moulded specimens.

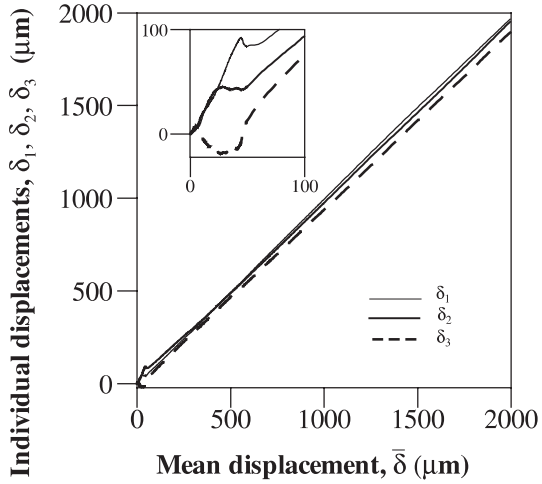

Fig. 3. Comparison of the individual LVDT readings.

obtained load and CMOD measurements. In order to examine the procedure for determining the σ–w curve and other parameters that could represent the toughening obtained with the fibres, the experimental response of the individual specimen is first analysed. Data from a typical test of a 150 × 150 mm cylinder with a 15 mm deep notch are considered.

4.1. The σ–w curve

As mentioned earlier, three individual CMOD (δ_i) measurements were obtained in the tests of the moulded cylinders. Typical load (P) versus δ_i curves are shown in Fig. 2, where each curve corresponds to one LVDT. It can be seen that the curves are similar over the entire test range, practically coinciding beyond a CMOD of about 100 μm. However, at smaller values of CMOD, as in the inset of Fig. 2, the individual measurements vary significantly. Such differences can be attributed to the non-symmetric crack propagation in the matrix, which can even result in some closure of the crack mouth (or negative CMOD) at crack initiation; e.g., the δ_3-readings in this case are initially negative indicating the closure of the notch mouth at this point. This aspect can be further seen in Fig. 3, where the δ_i-readings are plotted against the mean crack opening. Similar results have also been obtained by Casanova [3].

For obtaining the average CMOD, two measuring systems have been used: the three LVDTs placed between rings mounted on the specimen that give individual readings, which are averaged; and three extensometers mounted directly on the specimen giving an averaged signal. The average signals determined by the two measuring systems are compared in Fig. 4, where $\bar{\delta}$ is obtained from the extensometers and the mean δ_i is obtained by averaging the LVDT readings. It is clear that the mean response is practically identical over the whole range, implying that both types of measuring systems are equally satisfactory for measuring the average CMOD. The crack width, w, is then calculated from the average CMOD by subtracting the value at

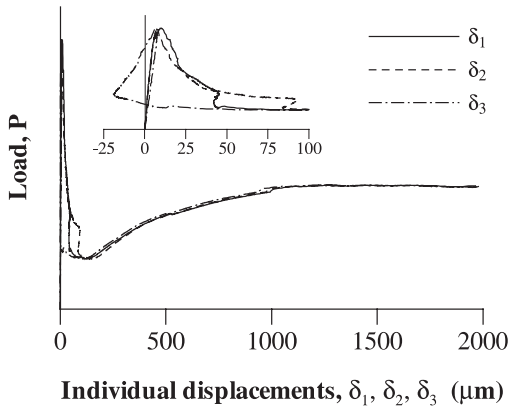

Fig. 2. Load versus δ_i diagrams from a typical test.

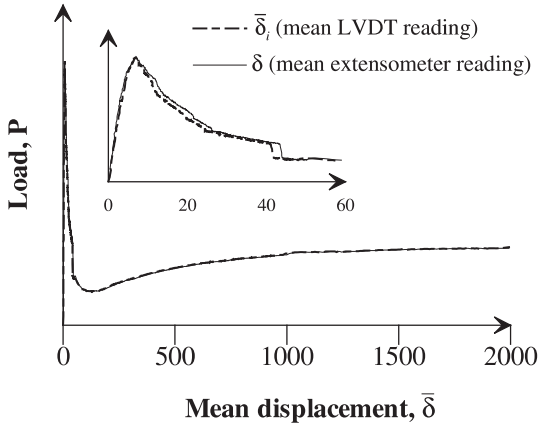

Fig. 4. Load versus mean crack-opening response.

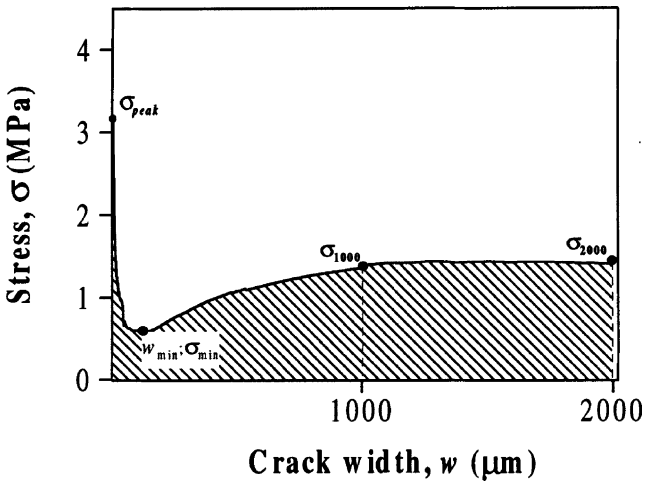

Fig. 5. The σ–w curve and other parameters.

peak load ($\bar{\delta}_{\text{peak}}$); i.e., $w = \bar{\delta} - \bar{\delta}_{\text{peak}}$, for $w \geqslant 0$, as in the RILEM Recommendation [1]. The load is divided by the net area (or the area of the unnotched ligament) to give the applied stress, σ. This leads to the curve shown in Fig. 5 corresponding to the data considered in Fig. 4.

4.2. Rotation of the crack faces

As seen in the previous section, there are significant differences in the individual LVDT readings for small $\bar{\delta}$, which implies some rotation of the crack faces with respect to each other. This can be attributed to non-symmetric fracture, with the crack starting from one or more points on the notch tip and propagating over the ligament. Such non-symmetric fracture has been observed previously and analysed, in significant detail, for double-edge notched panels by researchers such as Hordijk [9]. However, in the present case, detailed analysis is complicated since the crack propagation across the notch plane is two-dimensional.

Nevertheless, in order to evaluate the non-symmetry of the crack opening, the relative rotation of the crack faces has been calculated from the individual CMOD readings, δ_i. This is given by the angle between the vertical axis and the normal to a plane defined by the readings at any point in time (see inset of Fig. 6). Considering the readings δ_i of the three LVDTs located respectively at the coordinates (x_i, y_i), a relative crack opening plane can be defined as:

$$A(x - x_1) + B(y - y_1) + C(\delta - \delta_1) = 0 \tag{1}$$

where

$$A = \begin{vmatrix} y_2 - y_1 & \delta_2 - \delta_1 \\ y_3 - y_1 & \delta_3 - \delta_1 \end{vmatrix} \quad B = \begin{vmatrix} \delta_2 - \delta_1 & x_2 - x_1 \\ \delta_3 - \delta_1 & x_3 - x_1 \end{vmatrix}$$

$$C = \begin{vmatrix} x_2 - x_1 & y_2 - y_1 \\ x_3 - x_1 & y_3 - y_1 \end{vmatrix}$$

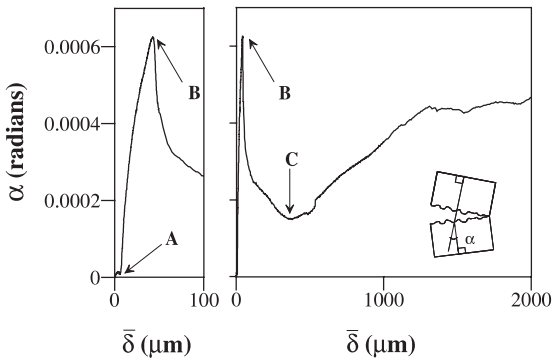

Fig. 6. Relative rotation of the crack faces during the test.

Accordingly, the rotation of the plane with respect to the axis of the specimen is given by:

$$\alpha = \tan^{-1}\left(\frac{\sqrt{A^2 + B^2}}{C}\right) \tag{2}$$

The evolution of the rotation in the test considered in the previous section can be seen in Fig. 6, with the rotations up to $\bar{\delta} = 100$ μm on the left and up to 1200 μm on the right. The trends are useful for explaining the behaviour of the specimen. It can be seen that there is some rotation up to peak load (marked as point A) that can be attributed to the heterogeneity of the specimen and imperfections in the test setup itself. The rotation at the peak load will be hereafter denoted as α_{peak}. More importantly, the rotation increases after the peak due to non-symmetric crack propagation until point B, where the matrix-dominated response is assumed to end. Thereafter, the crack faces are only bridged by the fibres, which are obviously distributed in a non-symmetric manner causing further rotation (beyond point C) as they are progressively stressed and pulled out. The maximum rotation ($\alpha_{\max}$), therefore, seems to be a good indication of the degree of non-symmetry in the test.

4.3. Stress and toughness parameters

For a quantitative analysis of the behaviour of the specimens considered in this study, several parameters have been defined in terms of the σ–w curve, as denoted in Fig. 5:

σ_{peak} is the first-peak stress, which basically corresponds to the matrix strength,
$\sigma_{\min}$ is the minimum stress reached after the post-peak drop,
$w_{\min}$ is the crack width corresponding to $\sigma_{\min}$,
σ_{1000} is the stress at a crack width of 1000 μm,
σ_{2000} is the stress at a crack width of 2000 μm.

Additionally, two other parameters also indicative of the material toughness have been considered. The first is an absolute toughness measure given by the area under the σ–w curve until a prescribed crack width limit (i.e., the shaded area in Fig. 5). This is based on the concept of fracture energy of plain concrete obtained as the area under the complete σ–w curve [10,11]. Using, therefore, similar notations, the absolute toughness is calculated as:

$$G_F^{w_{lim}} = \int_{w=0}^{w_{lim}} \sigma(w)\,dw \tag{3}$$

where w_{lim} is the limiting crack width until which the area is evaluated. Two limits have been considered here, $w = 1000$ and 2000 μm, which define G_F^{1000} and G_F^{2000}, respectively. Note that the $G_F^{w_{lim}}$-values can be considered as material parameters and are theoretically independent of the geometry or size of the specimen.

Another related parameter that is proposed is the equivalent tensile strength, denoted as $f_{eq}^{t,w_{lim}}$ and calculated as:

$$f_{eq}^{t,w_{lim}} = \frac{G_F^{w_{lim}}}{w_{lim}} \tag{4}$$

Note that $f_{eq}^{t,w_{lim}}$ is an average post-peak strength over a range of w (i.e., 0 to w_{lim}). The values of $f_{eq}^{t,w_{lim}}$ represent the post-cracking strength and can be used as a parameter in σ–w models such as the drop-constant model, where the response is given by a vertical drop from the tensile strength and a constant residual strength [12]. The value of w_{lim} can be chosen as the maximum crack width to be considered in the analysis.

4.4. Total and effective fibres across the crack

In addition to calculating the parameters discussed earlier, the fibres crossing the fracture plane of the specimen have been counted after each test. This was done in order to correlate the parameters obtained from each specimen to the number of fibers that bridge the crack. Moreover, many fibres do not contribute to the strength due to their being orientated almost parallel to the crack. Therefore, both the total number of fibers and the number of effective fibres have been identified through visual observation and counted. An effective fibre is assumed to be that which has been pulled out (as opposed to that which is simply exposed by the crack). In the present study, there is no ambiguity in such identification since the effective fibres appear with their ends straightened out while the hooked ends of the others remain intact.

5. Behaviour of the moulded cylinders

5.1. Specimen-to-specimen variability

As the first step in the analysis of the results, the variability of the experimentally obtained parameters is evaluated. Considering the 150 × 150 mm cylinders with 15 mm deep notches, the stress-crack opening curves obtained from five different tests are shown in Fig. 7. It can be seen that the residual stresses in the fiber-dominated response vary significantly from one specimen to another. The shape of the curve is considerably different just after the post-peak drop but later remains practically the same. From these curves, the mean values, standard deviations and coefficients of variation of several parameters have been obtained and are presented in Table 4. It can be seen that the first-peak stress or the tensile strength (σ_{peak}) ranges from 1.8 to 3.1 MPa, with a coefficient of variation of 20%, which seems to be higher than the normal range for the modulus of rupture of concrete. The minimum stress value (σ_{min}) also has a variability of the same order of magnitude while the corresponding displacement value (w_{min}) exhibits higher scatter. The high variability may be attributed to the relatively small critical section of the notched cylinder, where the resistance to crack initiation and propagation can differ considerably from one specimen to another. The parameters related to the rotations (i.e., α_{peak} and α_{max}) have much higher variations since they incorporate three different displacements. Nevertheless, the values of the rotations are quite small, not exceeding 1×10^{-5} rad (or 0.0006°) at the peak load and about 2×10^{-3} rad (or 0.11°) overall. No significant influence of the rotations on the post-peak response is, therefore, expected, especially at larger crack widths.

The post-peak stresses and other toughness parameters have variations of 20–30%, reflecting the differences

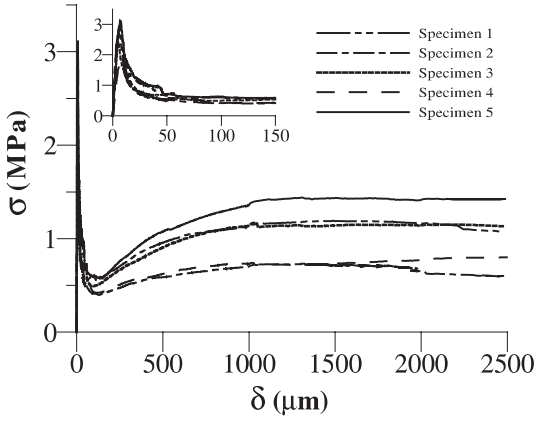

Fig. 7. Stress-crack opening curves of 150 × 150 mm cylinders with 15 mm deep notches.

Table 4
Parameters obtained for the specimens of 150 × 150 mm and 15 mm deep notch

Specimen	σ_{peak} (MPa)	σ_{min} (MPa)	w_{min} (μm)	α_{peak} (10^{-3} rad)	α_{max} (10^{-3} rad)	σ_{1000} (MPa)	σ_{2000} (MPa)	G_F^{1000} (N/mm)	G_F^{2000} (N/mm)	$f_{eq}^{t,1000}$ (MPa)	$f_{eq}^{t,2000}$ (MPa)	Fibres total/ Effective
1	2.7	0.51	41	0.022	2.05	1.1	1.2	0.91	2.08	0.91	1.04	66/37
2	3.0	0.40	122	0.024	0.58	0.7	0.7	0.60	1.32	0.60	0.66	45/21
3	2.4	0.49	85	0.039	0.67	1.2	1.1	0.88	2.02	0.88	1.01	73/41
4	1.8	0.42	120	0.089	1.77	0.7	0.8	0.62	1.36	0.62	0.68	59/23
5	3.1	0.58	125	0.019	0.63	1.4	1.4	1.03	2.46	1.03	1.23	66/47
Mean	2.6	0.48	99	0.038	1.14	1.0	1.0	0.81	1.84	0.81	0.92	62/34
Standard deviation	0.5	0.07	36	0.029	0.71	0.3	0.3	0.19	0.50	0.19	0.25	11/11
Coefficient of variation (%)	20	15	37	75	63	28	30	23	27	23	27	17/34

observed in the post-peak regime of the stress-crack opening curves. The parameters corresponding to the w_{lim} value of 1000 μm seem to have lower scatter than those determined for 2000 μm.

The fiber counts yield interesting results indicating that the number of fibers, on the relatively small cross-section of the specimen, can vary significantly, especially when the effective fibers are considered. In this set of five tests, the effective fibers range from 21 to 47, with the two extreme cases corresponding to the extremes in the values of the post-peak stresses and toughness parameters. This clearly indicates that the variability in the fiber-dominated response is produced basically by the randomness of the number of fibers bridging the crack. This aspect will be studied further later on considering all the specimens tested in this study.

It was found that the specimen-to-specimen variability in all the different sets of tests was similar and, therefore, only the average results are analysed hereafter. Nevertheless, the coefficients of variation of the different sets of tests are reported.

5.2. Effects of specimen slenderness on the response

The first series of tests within the parametric study was performed on moulded cylindrical specimens of 150 mm diameter with three different heights: 150, 300 and 450 mm (i.e., with $h/\varnothing$ of 1, 2 and 3, respectively), all with a 15 mm deep notch at mid-height. The average

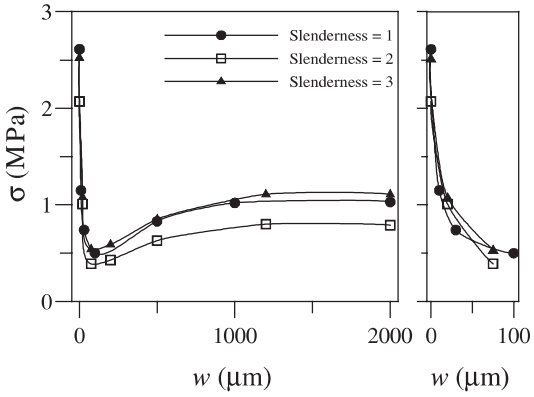

Fig. 8. Average σ–w curves for specimens with different slenderness ratios.

σ–w curves obtained for the three cases are shown in Fig. 8. It can be seen that there is no clear effect of the slenderness, with similar behaviour in all cases.

The values of the different stress and toughness based parameters obtained from the tensile response are given in Table 5. Again, no trend can be identified for the effect of slenderness on the mean values, especially when the inherent variability is considered. The lower values obtained for $h/\varnothing = 2$ can be attributed to the fewer fibres found, on average, across the cracks in these specimens. For the post-peak parameters, it seems that an increase in slenderness leads to an increase in the

Table 5
Parameters obtained for the specimens with different slenderness ratios (mean values and coefficients of variation in %)

$h/Ø$	σ_{peak} (MPa)	σ_{min} (MPa)	w_{min} (μm)	α_{peak} (10^{-3} rad)	α_{max} (10^{-3} rad)	σ_{1000} (MPa)	σ_{2000} (MPa)	G_F^{1000} (N/mm)	G_F^{2000} (N/mm)	$f_{eq}^{t,1000}$ (MPa)	$f_{eq}^{t,2000}$ (MPa)	Fibres total/ Effective
1	2.6	0.48	99	0.038	1.14	1.0	1.0	0.81	1.84	0.81	0.92	62/34
	±20%	±15%	±37%	±75%	±63%	±28%	±30%	±24%	±27%	±23%	±27%	±17%/±34%
2	2.1	0.30	94	0.047	0.81	0.7	0.7	0.60	1.34	0.60	0.67	48/25
	±7%	±16%	±64%	±22%	±40%	±41%	±38%	±36%	±38%	±35%	±37%	±14%/±35%
3	2.5	0.51	126	0.049	0.77	1.1	1.1	0.84	1.96	0.84	0.98	70/41
	±5%	±30%	±33%	±42%	±20%	±42%	±44%	±38%	±40%	±38%	±41%	±36%/±38%

coefficients of variation, with the parameters corresponding to $h/\varnothing = 1$ generally exhibiting the least scatter. Again, the toughness parameters corresponding to the w_{lim} value of 1000 μm exhibit less variability than those calculated for 2000 μm.

The relative crack face rotations have also been computed, and the corresponding rotation at the peak (α_{peak}) and the maximum rotation during the test (α_{max}) are presented in Table 5. A clear effect of the slenderness can be observed in the case of the relative rotation at peak stress, with α_{peak} increasing with an increase in slenderness, as can be expected due to decrease in the flexural stiffness of the specimen. However, the values are very small (i.e., less than 5×10^{-5} rad) compared to the maximum rotation α_{max}, which interestingly decreases, though slightly, with an increase in slenderness. The order of magnitude of the maximum rotation seems to be about 1×10^{-3} rad.

5.3. Effects of notch depth

Considering the 150×150 mm specimen, the notch depth was varied in the second series as 10, 15 and 20 mm. The corresponding average σ–w curves are shown in Fig. 9. It can be observed that, in general, the behaviour is similar, with the 20 mm notch specimens exhibiting a steeper drop after the peak.

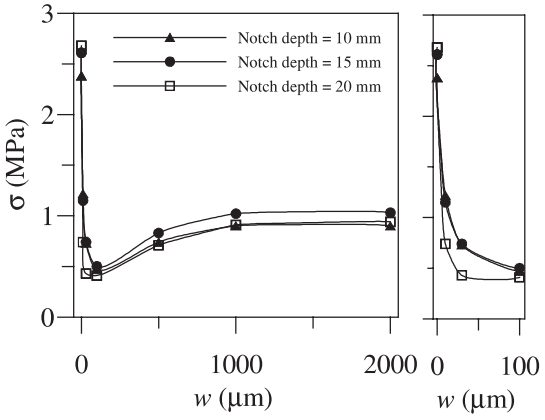

Fig. 9. Average σ–w curves for specimens with different notch depths.

Table 6 gives the mean values and the coefficients of variation of the parameters obtained for each notch depth. It can be observed that the notch depth influences the peak stress slightly, with a higher maximum stress for deeper notches. Also, specimens with 20 mm notches exhibit almost 35% lower σ_{min}-values with respect to those with 15 mm notches. However, there is no significant difference in this respect between the specimens with 10 and 15 mm notches. On the other hand, w_{min}-values decrease significantly with an increase in notch depth reflecting the steeper post-peak drops, which may be attributed to higher stress concentrations. The relative rotation of the crack faces at peak stress, α_{peak}, is found to decrease as the notch depth increases while α_{max} is almost constant at about $1–2 \times 10^{-3}$ rad. The trends in $G_F^{w_{lim}}$ and, consequently, in the equivalent tensile strengths are practically independent of the notch depth, with slightly higher values for the notch depth of 15 mm.

Considering the above results and the fact that shallower notches may lead to the crack initiation outside the notch [13], the 15 mm deep notch appears to be acceptable.

5.4. Relation between the response and the number of effective fibres

It was already seen that the variability in the post-peak stress and toughness parameters could be explained by the randomness in the number of effective fibres across the crack. This is further examined in order to be able to justify the large scatter observed in the results. Accordingly, the values of four representative parameters (i.e., $\sigma_{peak}, \sigma_{min}, \sigma_{2000}$ and $f_{eq}^{t,2000}$) obtained from all the tests considered in the previous sections are plotted in Figs. 10–13 with respect to the number of effective fibres. As mentioned earlier, the effective fibres are those that have been pulled out as indicated by the straightening of the hooked ends.

In the case of the peak stress, σ_{peak}, there is no trend (see Fig. 10) with respect to the effective fibre count confirming that this parameter is dominated by the matrix behaviour. In the case of σ_{min} (see Fig. 11), there is some dependence of the minimum stress on the fibre count indicating the combined influence of the matrix

Table 6
Parameters obtained for the specimens with different notch depths (mean values and coefficients of variation in %)

Notch depth (mm)	σ_{peak} (MPa)	σ_{min} (MPa)	w_{min} (μm)	α_{peak} (10^{-3} rad)	α_{max} (10^{-3} rad)	σ_{1000} (MPa)	σ_{2000} (MPa)	G_F^{1000} (N/mm)	G_F^{2000} (N/mm)	$f_{eq}^{t,1000}$ (MPa)	$f_{eq}^{t,2000}$ (MPa)	Fibres total/ Effective
10	2.4	0.45	115	0.059	1.46	0.9	0.9	0.72	1.66	0.72	0.83	58/33
	±26%	±20%	±29%	±44%	±18%	±19%	±21%	18%	±19%	±17%	±18%	±20%/±21%
15	2.6	0.48	99	0.038	1.14	1.0	1.0	0.81	1.84	0.81	0.92	62/34
	±20%	±15%	±37%	±75%	±63%	±28%	±30%	±24%	±27%	±23%	±27%	±17%/±34%
20	2.7	0.36	63	0.030	1.60	0.9	0.9	0.69	1.64	0.69	0.82	45/27
	±9%	±9%	±59%	±65%	±37%	±23%	±21%	±20%	±20%	±20%	±20%	±18%/±16%

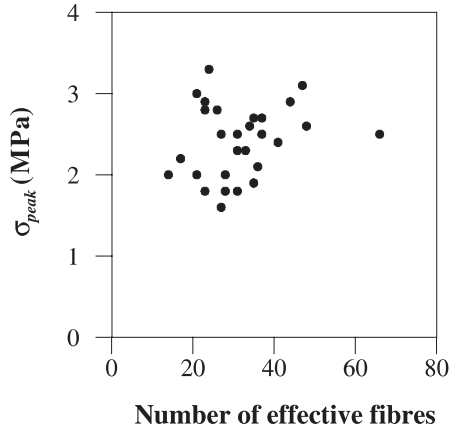

Fig. 10. Values of σ_{peak} versus the number of effective fibres.

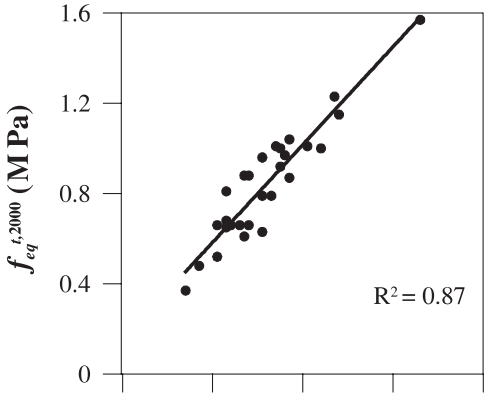

Fig. 13. Values of $f_{eq}^{t,2000}$ versus the number of effective fibres.

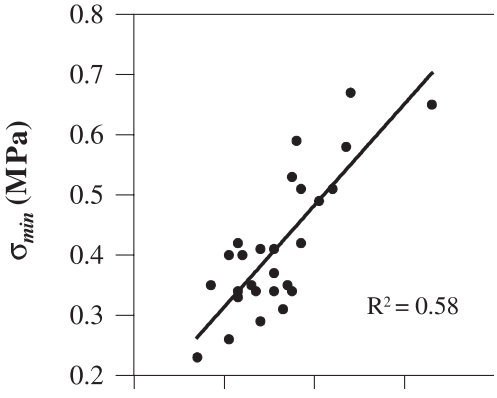

Fig. 11. Values of σ_{min} versus the number of effective fibres.

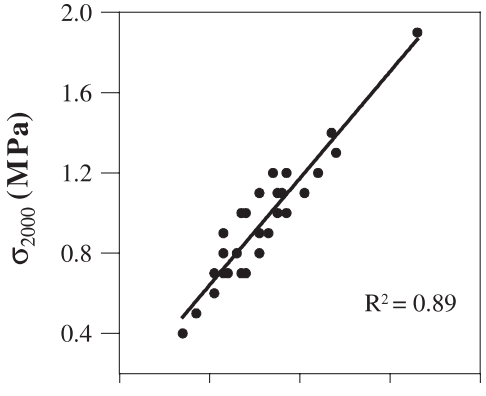

Fig. 12. Values of σ_{2000} versus the number of effective fibres.

and the fibres on the behaviour, at this stage. Note that the line shown in the plot is a linear least squares fit of the data points and R^2 is the coefficient of determination for the regression.

More importantly, there is a linear dependence of the post-peak parameters, σ_{2000} and $f_{eq}^{t,2000}$, on the number of effective fibres, as seen in Figs. 12 and 13. This correlation explains the source of the large variability in the toughness results. The linear dependence of the post-peak parameters on the number of fibers that bridge the crack or the density of fibres can be used to define more reliable material parameters if a correlation can be established for different types of concrete and fibre. However, it would be more interesting for practical applications to correlate the tensile behaviour to the total number of fibers across a crack plane, which can be estimated by models such as that of Stroeven [14] from the quantity of fibres in the concrete. Along these lines, the total and effective fibres observed on the crack planes of all the specimens with a notch depth of 15 mm are plotted in Fig. 14. It can be seen that there is a reasonable correlation between the two, with about 63 effective fibres for every 100 fibres on the crack plane. The trend observed implies that further and more extensive studies could possibly yield relations between the post-peak behaviour of the fiber concrete and the dosage of fibres.

6. Behaviour of cored specimens

The test methodology considered here can be applied not only to "virgin" moulded cylinders but also cores extracted from existing structures. In order to illustrate this possibility, cylindrical cores with a diameter of 93 mm were extracted from $150 \times 150 \times 600$ mm prisms that had been cast along with the moulded cylinders. The extraction was performed along the direction of the filling (or casting) of the prism and perpendicular to it,

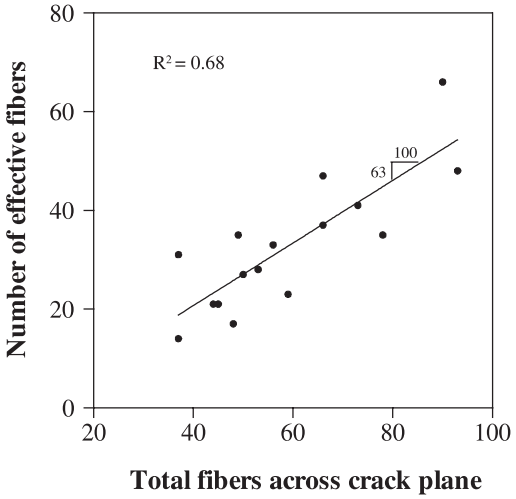

Fig. 14. Total versus number of effective fibres.

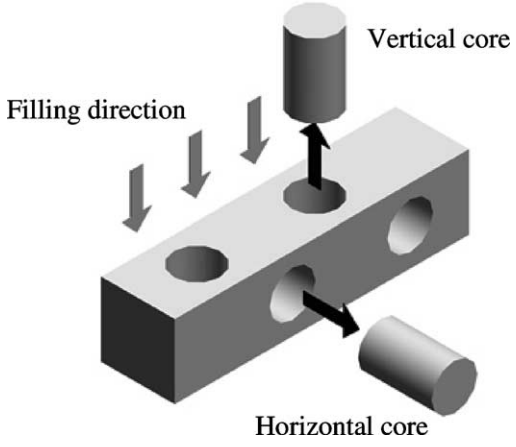

Fig. 15. Extraction of cores.

as shown in Fig. 15. Since the prisms had been compacted by table vibration, the fibres are expected to be oriented preferentially along horizontal planes [15]. Therefore, the response of the core would depend significantly on its original orientation with respect to the casting direction. Obviously the prisms used here are not representative of real-scale elements but have been used to draw attention to the importance of the fibre orientation on the mechanical response. For a more detailed analysis, cores should be extracted from actual structural elements to evaluate the orientation effects.

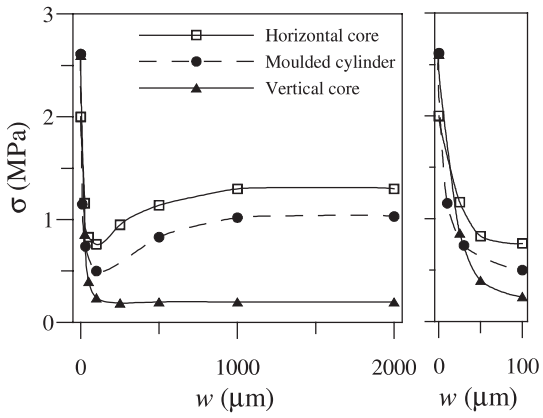

Fig. 16. Average σ–w curves of cores and moulded cylinders.

The cores were cut to a height of 100 mm and a 9.3 mm circumferential notch was cut in each of them at mid-height. Fig. 16 shows the average σ–w responses for the cores extracted in each direction. It can be clearly seen that cores obtained vertically (i.e., along the casting direction) yield lower post-peak strengths than those extracted horizontally. The better response of the horizontal cores can be attributed to most of the fibres being oriented perpendicular to the crack plane. Similar results have also been reported by Casanova [3].

Along with the mean results of the cores, the curve corresponding to the moulded 150×150 mm cylinders is plotted as a reference. Note that the slenderness ratio is about one and the notch depth is 10% of the cylinder diameter in all the cases. It can be seen that the response of the cylinder that is compacted in a mould by tamping lies closer to that of the horizontal cores and exhibits a similar trend with lower residual strengths. This implies that stronger fibre orientation in the horizontal cores leads to higher toughness than in the moulded cylinders. Therefore, the behaviour of the moulded cylinder (compacted by manual tamping, without energetic vibration), with an isotropic fibre orientation, gives a conservative estimate of the behaviour of concrete with fibres oriented preferentially along the direction of the principal stress.

The stress and toughness parameters of the cores are given in Table 7, again demonstrating the poorer post-peak response of the vertical cores. The number of fibres

Table 7
Parameters obtained for the cores (mean values and coefficients of variation in %)

Core orientation	σ_{peak} (MPa)	σ_{min} (MPa)	w_{min} (μm)	σ_{1000} (MPa)	σ_{2000} (MPa)	G_F^{1000} (N/mm)	G_F^{2000} (N/mm)	$f_{eq}^{t,1000}$ (MPa)	$f_{eq}^{t,2000}$ (MPa)	Fibres total/ Effective
Vertical	2.6 ±9%	0.19 ±28%	293 ±40%	0.2 ±26%	0.2 ±30%	0.26 ±23%	0.48 ±23%	0.26 ±23%	0.24 ±24%	18/3 ±32%/±59%
Horizontal	2.0 ±17%	0.74 ±18%	90 ±38%	1.3 ±24%	1.3 ±26%	1.11 ±23%	2.46 ±23%	1.11 ±22%	1.23 ±24%	28/13 ±38%/±54%

seen on the crack faces in each case also reflects the preferential orientation of the fibres. The larger number of effective fibres leads to hardening-type behaviour after the post-peak drop and higher toughness.

From a practical point of view, it is useful that the same test method can be used for the characterisation of "virgin" material through moulded specimens and of the material within an existing structure. However, the coring direction should be taken into account, especially in the case of elements that have been compacted by energetic vibration, in the interpretation of results from tests on cores. On the other hand, the extraction of cores in several directions would permit the evaluation of the existence of preferentially-oriented fibres due to the compaction process and the effect of this phenomenon on the tensile behaviour, as demonstrated by Casanova [3] and Rossi [16].

7. Conclusions and final considerations

The study demonstrates that, for the ranges used of the parameters and the limited number of specimens tested here, the uniaxial tensile test for SFRC, using a notched moulded cylinder, proposed recently as a RILEM Draft Recommendation, is robust and representative of the material response. No significant influences of the geometrical characteristics of the specimen or problems of instability due to the loss of control were encountered in the test. There is some relative rotation between the crack faces, especially during the initial part of the post-peak response, which is attributed to the non-symmetric crack propagation in the matrix. In most of the cases, the rotation decreases in the later part of the post-peak regime, which is dominated by the fibre response. Nevertheless, the influence of the rotation on the post-peak stress-crack width response of fibre concrete is expected to be negligible.

The post-peak stresses and toughness parameters obtained from the tests exhibit coefficients of variation of up to 30%. The significant scatter is mainly attributed to the randomness of the number of effective fibres bridging the crack, considering the relatively small cross-section of the specimen.

The test methodology has also been employed for the characterisation of the tensile response of cores extracted from cast SFRC elements. However, the effect of the fibre orientation on the response can be significant and has to be taken into account, especially when energetic vibration has been used for compacting the SFRC element.

Toughness measures based on the post-peak response have been proposed for representing the tensile behaviour of SFRC, and for possible use in structural analysis and design. Among the parameters determined here, the equivalent tensile strength seems to be a promising concept, which is readily applicable in simple constitutive models.

An important issue that is worth discussing is the comparison of the tensile test with the flexural test, which is much more popular. Obviously, the latter is much easier to perform and seems to provide a flexural strength and toughness parameters with much lower variability. This suggests that the tensile test would be applied in a more limited context, probably when the σ–w relation of the material is required, for example, to compare the performance of different types of fibres or to provide the input for finite element based structural analysis.

Acknowledgements

Partial financial support was provided by the European Commission Contract BRPR.CT98.0813 for the Brite project "Test and design methods for steel fibre reinforced concrete", and by the Spanish CICYT through grants PB98-0298 and MAT99-1370-CE to the UPC. The other partners of the Brite project are Bekaert (coordinator), Balfour Beatty, Belgian Building Research Institute, Catholic University of Leuven, FCC Construcción, Ruhr-University of Bochum, SIBO-Gruppe GmbH, Technical University of Braunschweig, Technical University of Denmark and University of Wales-Cardiff. The doctoral studies of B.E. Barragán at the UPC were funded by CONICET (Argentina). The materials used in this work were donated by Bekaert, Cementos Molins and Grace.

References

[1] RILEM TC 162. Test and design methods for steel fibre reinforced concrete: Uniaxial tension test for steel fibre reinforced concrete. Mater Struct 2001;34(235):3–6.
[2] Wang Y, Li VC, Backer S. Experimental determination of tensile behavior of fiber reinforced concrete. ACI Mater J 1990; 87(5):461–8.
[3] Casanova P. Bétons renforcés de fibres métalliques: du matériauàla structure. Doctoral thesis, école Nationale des Ponts et Chaussées, Paris, 1995.
[4] Groth P, Noghabai K. Fracture mechanics properties of steel fibre-reinforced high-performance concrete. In: de Larrard F, Lacroix R, editors. Utilization of High-strength/ High-performance Concrete. Paris: Presses de l'Ecole Nationale des Ponts et Chaussées; 1996. p. 747–56.
[5] Rossi P. High performance multimodal fiber reinforced cement composites (HPMFRCC): The LCPC experience. ACI Mater J 1997;94(6):478–83.
[6] Stang H, Bendixen S. A simple model for uniaxial testing of fiber reinforced concrete. In: Allison IM, Balkema AA, editors. Experimental mechanics, advances in design, testing and analysis. Rotterdam; 1998. p. 887–92.
[7] Stang H. Uniaxial tension testing of fibre reinforced concrete. Report on Test and Design Methods for Steel Fibre Reinforced concrete. EU Contract BRPR-CT98-813, Subtask 2.1. Definition of round robin testing. Department of Structural

Engineering and Materials, Technical University of Denmark, Lyngby, 1999.
[8] Hillerborg A, Modeér M, Petersson PE. Analysis of crack formation and crack growth in concrete by means of fracture mechanics and finite elements. Cem Concr Res 1976;6:773–82.
[9] Hordijk DA. Local approach to fatigue of concrete. Doctoral thesis, Delft University of Technology, Delft, 1991.
[10] Petersson PE. Fracture energy of concrete: Method of determination. Cem Concr Res 1980;10:79–89.
[11] Hillerborg A. Determination and significance of the fracture toughness of steel fibre concrete. In: Shah SP, Skarendahl Å, editors. Steel Fiber Concrete. London: Elsevier Applied Science Publishers; 1986. p. 257–71.
[12] Olesen JF, Stang H. Designing FRC slabs on grade for temperature and shrinkage induced cracks. In: Rossi P, Chanvillard G, editors. Fibre-Reinforced Concretes. France: RILEM, Cachan; 2000. p. 337–46.
[13] Barragán BE. Failure and toughness of steel fiber reinforced concrete under tension and shear. Doctoral thesis, Universitat Politècnica de Catalunya, Barcelona, Spain, 2002.
[14] Stroeven P. Analysis of fibre distributions in fibre reinforced materials. J Microscopy 1977;111:283–95.
[15] Saldivar H. Flexural Toughness characterization of steel fiber reinforced concrete. Doctoral thesis, Universitat Politècnica de Catalunya, Barcelona, Spain, 1999.
[16] Rossi P. Les bétons de fibres métalliques. Paris: Presses de l'Ecole Nationale des Ponts et Chaussees; 1998.